

## Effect of Different Al<sub>2</sub>O<sub>3</sub> Supports on the Synthesis of Tetralin by Selective Catalytic Hydrogenation of Naphthalene

Xiao-Ping Su,<sup>✉</sup> Le Zhao,<sup>a</sup> Xiang-Tong Wang,<sup>a</sup> Zhao Wang,<sup>a</sup> Zhi-Chao Wang,<sup>a</sup>  
Tao Shen<sup>a</sup> and Ping Zhang<sup>\*,a</sup>

<sup>a</sup>School of Chemical Engineering, Northwest Minzu University,  
Key Laboratory of Environment-Friendly Composites of the State Ethnic Affairs Commission,  
Gansu Provincial Biomass Function Composites Engineering Research Center,  
Key Laboratory for Utility of Environment-Friendly Composites and Biomass,  
Universities of Gansu Province, Lanzhou 730030, Gansu, China

Different Al<sub>2</sub>O<sub>3</sub> carriers were synthesized by co-precipitation and sol-gel method. From them, 4%NiO-20%MoO<sub>3</sub>/Al<sub>2</sub>O<sub>3</sub> catalysts were prepared by incipient wetness impregnation. The catalysts were characterized by X-ray diffraction analysis (XRD), N<sub>2</sub> adsorption-desorption, NH<sub>3</sub>-temperature programmed desorption (TPD) and H<sub>2</sub>-temperature programmed reduction (TPR) and subsequently used for selective hydrogenation of naphthalene to high-value tetralin. The results showed that Ni-Mo/so-ge Al<sub>2</sub>O<sub>3</sub> (900) exhibited better catalytic performance than Ni-Mo/commercial Al<sub>2</sub>O<sub>3</sub>, achieving 99.56% naphthalene conversion and 99.43% tetralin selectivity.

**Keywords:** Al<sub>2</sub>O<sub>3</sub>, catalyst, naphthalene, tetralin, selective hydrogenation

### Introduction

Naphthalene hydrogenation has been widely reported.<sup>1-3</sup> Active metals such as Co, Mo, Ni, W, Pt, Pd, Ru, Ni-Mo, Ni-W and Co-Mo loaded on Al<sub>2</sub>O<sub>3</sub>, SiO<sub>2</sub>, TiO<sub>2</sub>, HY zeolite, HZSM-5 zeolite, activated carbon, Al<sub>2</sub>O<sub>3</sub>/SiO<sub>2</sub>, and Al<sub>2</sub>O<sub>3</sub>/TiO<sub>2</sub> carriers have been used to study naphthalene hydrogenation.<sup>4-6</sup> Usually, noble metal catalysts have higher activity.<sup>7</sup> However, due to the lower cost and wider application, scholars focus more on transition metal catalysts,<sup>8</sup> especially Ni-Mo catalysts.<sup>9,10</sup> Although the price of tetralin is higher than that of decaline, most studies are devoted to the complete hydrogenation of naphthalene to decalin. Tetralin is an important solvent and chromatographic reagent.<sup>11-13</sup> Han and co-workers<sup>14</sup> used Fe-Mo based catalyst to produce tetralin and the highest yield of tetralin was 85%. Additionally, 84.9% tetralin yield was achieved by 4.2% Ni nano-clusters supported on MFI nano-sheets zeolite.<sup>15</sup>

In a preliminary research<sup>16</sup> carried out by some of us, the optimum active metal, metal loadings, loading ratio and reaction conditions for the naphthalene

selective hydrogenation to high-value tetralin have been determined. The present paper mainly investigates the effect of different Al<sub>2</sub>O<sub>3</sub> supports on the performance of 4%NiO-20%MoO<sub>3</sub>/Al<sub>2</sub>O<sub>3</sub> catalysts under the same reaction conditions employed in the preliminary studies.<sup>16</sup> It is well-established that carriers play an important role in catalysts, but there is little literature on the effects of Al<sub>2</sub>O<sub>3</sub> supports. This paper provides a reference study about the effects of different Al<sub>2</sub>O<sub>3</sub> supports on the synthesis of tetralin by naphthalene hydrogenation.

### Experimental

#### Preparation of catalysts

Al<sub>2</sub>O<sub>3</sub> was synthesized by a co-precipitation method,<sup>17</sup> in which 20 g of AlCl<sub>3</sub>·6H<sub>2</sub>O (Shanghai Aladdin Biochemical Technology Co., Ltd, Shanghai, China) and 10 g NaOH (Shanghai Aladdin Biochemical Technology Co., Ltd, Shanghai, China) were fully dissolved in deionized water. The NaOH solution was then slowly dropped into the AlCl<sub>3</sub> solution with stirring. Subsequently, the obtained white precipitate, Al(OH)<sub>3</sub>, was vacuum filtered, rinsed with hot water, dried at 120 °C for 4 h and calcined at 600, 700, 800 and 900 °C for 4 h to produce Al<sub>2</sub>O<sub>3</sub>. Finally, the obtained

\*e-mail: 382106410@qq.com

Editor handled this article: Jaísa Fernandes Soares

Al<sub>2</sub>O<sub>3</sub> powders were pelletized and sieved (80-120 mesh), and then denoted as co-pr Al<sub>2</sub>O<sub>3</sub> (600), co-pr Al<sub>2</sub>O<sub>3</sub> (700), co-pr Al<sub>2</sub>O<sub>3</sub> (800) and co-pr Al<sub>2</sub>O<sub>3</sub> (900).

Al<sub>2</sub>O<sub>3</sub> was synthesized by the sol-gel method using 0.2 mol L<sup>-1</sup> Al(NO<sub>3</sub>)<sub>3</sub> (Sichuan South China Inorganic salt Co., Ltd, Sichuan, China) as aluminum source and Triton X-100 (Shanghai Aladdin Biochemical Technology Co., Ltd, Shanghai, China) as a dispersing agent.<sup>18</sup> Triton X-100 (60 drops) was added into 300 mL of the Al(NO<sub>3</sub>)<sub>3</sub> solution, and 2 mol L<sup>-1</sup> (NH<sub>4</sub>)<sub>2</sub>CO<sub>3</sub> (Sichuan South China Inorganic salt Co., Ltd, Sichuan, China) solution was slowly dropped into the mixture while stirring until pH 9. Subsequently, the mixture was vacuum filtered and then washed with hot deionized water. The precipitate was then refluxed in *n*-butanol for 2 h, dried at 120 °C for 4 h, and calcined at 800, 900, 1000 and 1100 °C for 4 h. Finally, the obtained Al<sub>2</sub>O<sub>3</sub> powders were pelletized and sieved (80-120 mesh), and then were denoted as so-ge Al<sub>2</sub>O<sub>3</sub> (800), so-ge Al<sub>2</sub>O<sub>3</sub> (900), so-ge Al<sub>2</sub>O<sub>3</sub> (1000) and so-ge Al<sub>2</sub>O<sub>3</sub> (1100).

Commercial Al<sub>2</sub>O<sub>3</sub> with saturated water absorption of 38 wt.% was purchased from the Aluminum Corporation of China Limited (Shanghai, China). Table 1 shows its physical and chemical properties.

4%NiO-20%MoO<sub>3</sub>/Al<sub>2</sub>O<sub>3</sub> catalysts were prepared by incipient wetness impregnation using Ni(NO<sub>3</sub>)<sub>2</sub>·6H<sub>2</sub>O and (NH<sub>4</sub>)<sub>6</sub>Mo<sub>7</sub>O<sub>24</sub>·4H<sub>2</sub>O as precursors. After immersion for 12 h, they were dried at 120 °C and calcined at 500 °C for 4 h. Finally, the obtained catalysts were denominated as Ni-Mo/commercial Al<sub>2</sub>O<sub>3</sub>, Ni-Mo/co-pr Al<sub>2</sub>O<sub>3</sub> (x, x = 600,

700, 800, 900) and Ni-Mo/so-ge Al<sub>2</sub>O<sub>3</sub> (y, y = 800, 900, 1000, 1100).

#### Characterization of catalysts

Al<sub>2</sub>O<sub>3</sub> was identified by using a Rigaku D/max-2400X (Tokyo, Japan) X-ray diffraction equipment using Cu Kα radiation. N<sub>2</sub> adsorption-desorption experiments were performed by a Quantachrome NOVA 2200e instrument (Florida, USA). The NH<sub>3</sub>-temperature programmed desorption (TPD) and H<sub>2</sub>-temperature programmed reduction (TPR) analysis of the catalysts was carried out on a TP-5080 device (Tianjin, China) with thermal conductivity detector.<sup>19</sup>

#### Catalytic performance

2 g catalyst and 1 g naphthalene were added to 19 g of *n*-hexane as a solvent in a stainless-steel batch reactor, employing 6 MPa of H<sub>2</sub> as a reductant. The solution was then mechanically stirred and heated to 200 °C for 8 h. The product was analyzed by the use of a 3420A gas chromatograph (Beifen, Beijing, China).

## Results and Discussion

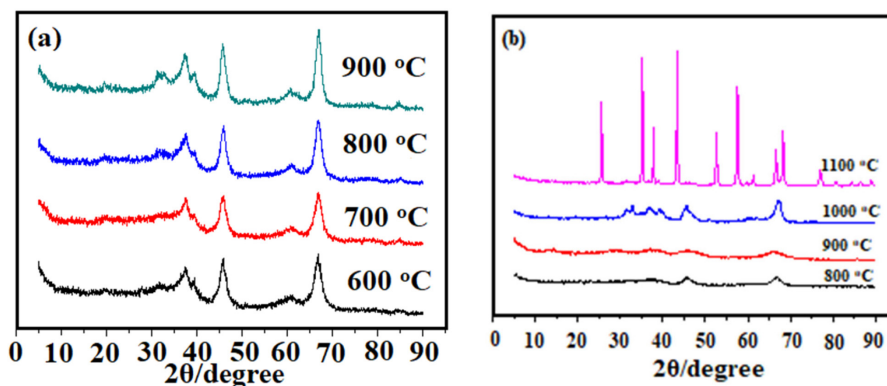
#### X-ray diffraction analysis (XRD)

Figure 1 shows the XRD patterns of Al<sub>2</sub>O<sub>3</sub> prepared by different methods. In Figure 1a, the diffraction peaks

**Table 1.** Physical and chemical properties of the commercial Al<sub>2</sub>O<sub>3</sub> support

Support	Physical properties			Distribution of acid strength / %		
	BET / (m <sup>2</sup> g <sup>-1</sup> )	Pore volume / (cm <sup>3</sup> g <sup>-1</sup> )	Pore diameter / nm	Weak (< 200 °C)	Middle (200-400 °C)	Strong (> 400 °C)
Al <sub>2</sub> O <sub>3</sub>	148.85	0.24	3.78	27.46	52.43	20.11

BET: Brunauer-Emmett-Teller.



**Figure 1.** XRD patterns of Al<sub>2</sub>O<sub>3</sub> prepared by (a) co-precipitation; (b) sol-gel method.

of  $\text{Al}_2\text{O}_3$  prepared by co-precipitation at the calcination temperature of 600, 700, 800 and 900 °C are basically similar, with three well-defined peaks around  $2\theta = 37, 45$  and  $67^\circ$  assigned to the characteristic peaks of  $\gamma\text{-Al}_2\text{O}_3$ .<sup>20</sup> The intensity of the diffraction peaks increased slightly with increasing calcination temperature. When the calcination temperature was 900 °C, two peaks appeared near  $2\theta = 32$  and  $40^\circ$ , which were assigned to the characteristic peaks of  $\theta\text{-Al}_2\text{O}_3$ . Therefore, when the calcination temperature rises to 900 °C,  $\text{Al}_2\text{O}_3$  prepared by co-precipitation method begins to transform from the  $\gamma$  phase to the  $\theta$  phase. In Figure 1b, the diffraction peaks of  $\text{Al}_2\text{O}_3$  prepared by the sol-gel method became sharper with increasing calcination temperature. At the temperature of 800 °C, the peaks around  $2\theta = 45$  and  $67^\circ$  appeared with low intensity, indicating that the  $\text{Al}_2\text{O}_3$  was in an amorphous form.<sup>21</sup> When the calcination temperature reached 900 °C, the characteristic peaks of  $\gamma\text{-Al}_2\text{O}_3$  became more obvious. At 1000 °C, the characteristic peaks of  $\theta\text{-Al}_2\text{O}_3$  ( $2\theta = 32, 38, 40^\circ$ ) appeared,<sup>22</sup> while at 1100 °C, the characteristic peaks of  $\alpha\text{-Al}_2\text{O}_3$  ( $2\theta = 26, 35, 38, 44, 53, 58, 68^\circ$ ) were clearly seen.<sup>23</sup>

#### $\text{N}_2$ adsorption-desorption

Figure 2 shows  $\text{N}_2$  adsorption-desorption isotherms and pore size distribution of different Ni-Mo/ $\text{Al}_2\text{O}_3$  catalysts. It can be observed that all isotherms are type IV, suggesting the presence of well-structured mesoporous materials.<sup>24,25</sup> Table 2 lists Brunauer-Emmett-Teller surface

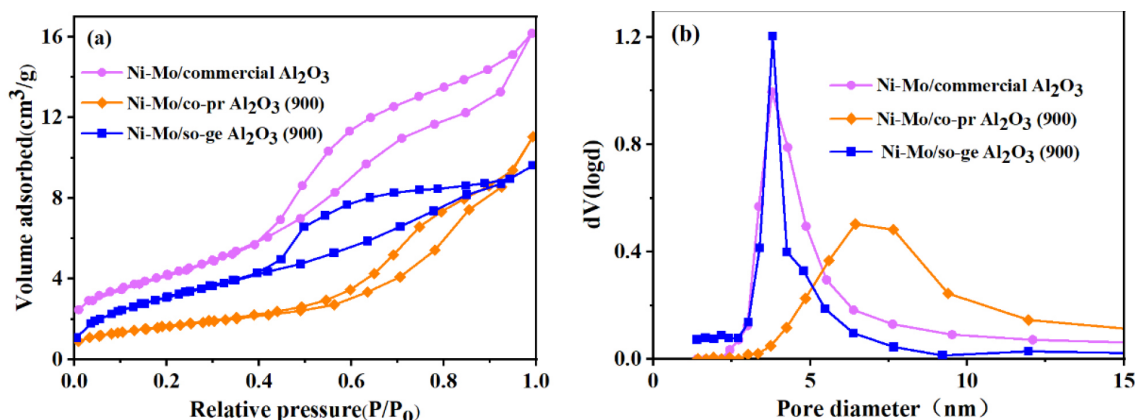


**Figure 2.**  $\text{N}_2$  adsorption-desorption isotherms (a) and pore size distribution (b) of different Ni-Mo/ $\text{Al}_2\text{O}_3$  catalysts.

**Table 2.** Textural properties of different Ni-Mo/ $\text{Al}_2\text{O}_3$  catalysts

Catalyst	$S_{\text{BET}} / (\text{m}^2 \text{g}^{-1})$	$V_{\text{total}} / (\text{cm}^3 \text{g}^{-1})$	Average pore size / nm
Ni-Mo/commercial $\text{Al}_2\text{O}_3$	114.93	0.17	5.98
Ni-Mo/Co-pr $\text{Al}_2\text{O}_3$ (900)	102.35	0.23	6.44
Ni-Mo/So-ge $\text{Al}_2\text{O}_3$ (900)	206.70	0.20	3.81

$S_{\text{BET}}$ : Brunauer-Emmett-Teller surface area;  $V_{\text{total}}$ : total pore volume.

areas ( $S_{\text{BET}}$ ), total pore volumes ( $V_{\text{total}}$ ), and average pore sizes for different Ni-Mo/ $\text{Al}_2\text{O}_3$  catalysts. The BET data for  $\text{Al}_2\text{O}_3$  catalysts is consistent with published results.<sup>26</sup> By comparison,  $S_{\text{BET}}$  of Ni-Mo/co-pr  $\text{Al}_2\text{O}_3$  is the smallest, while the  $S_{\text{BET}}$  of Ni-Mo/so-ge  $\text{Al}_2\text{O}_3$  is the largest, reaching  $206.70 \text{ m}^2 \text{g}^{-1}$ . Compared with Ni-Mo/commercial  $\text{Al}_2\text{O}_3$ ,  $V_{\text{total}}$  of Ni-Mo/co-pr  $\text{Al}_2\text{O}_3$  and Ni-Mo/so-ge  $\text{Al}_2\text{O}_3$  was increased by 17.6 and 30.0%, respectively. Average pore sizes of Ni-Mo/commercial  $\text{Al}_2\text{O}_3$ , Ni-Mo/co-pr  $\text{Al}_2\text{O}_3$  and Ni-Mo/so-ge  $\text{Al}_2\text{O}_3$  are 5.98, 6.44 and 3.81 nm, respectively.

#### $\text{NH}_3$ -TPD

According to the desorption temperature, the acid sites can be divided into weak ( $< 200^\circ\text{C}$ ), medium ( $200\text{-}400^\circ\text{C}$ ), and strong ( $> 400^\circ\text{C}$ ). Figure 3 shows  $\text{NH}_3$ -TPD curves and acid strength distribution of different Ni-Mo/ $\text{Al}_2\text{O}_3$  catalysts. Ni-Mo/ $\text{Al}_2\text{O}_3$  is mainly medium-weak acid.<sup>27</sup> By comparison, total acidity of Ni-Mo/so-ge  $\text{Al}_2\text{O}_3$  is the largest, while total acidity of Ni-Mo/co-pr  $\text{Al}_2\text{O}_3$  is the smallest, which may be due to the largest  $S_{\text{BET}}$  of Ni-Mo/so-ge  $\text{Al}_2\text{O}_3$  that reflects more surface active sites.

#### $\text{H}_2$ -TPR

Figure 4 presents the  $\text{H}_2$ -TPR profiles of different Ni-Mo/ $\text{Al}_2\text{O}_3$  catalysts, showing two reduction peaks attributed to the reduction of Mo species (lower temperatures) and  $\text{NiAl}_2\text{O}_4$  species (higher temperature reduction peaks),

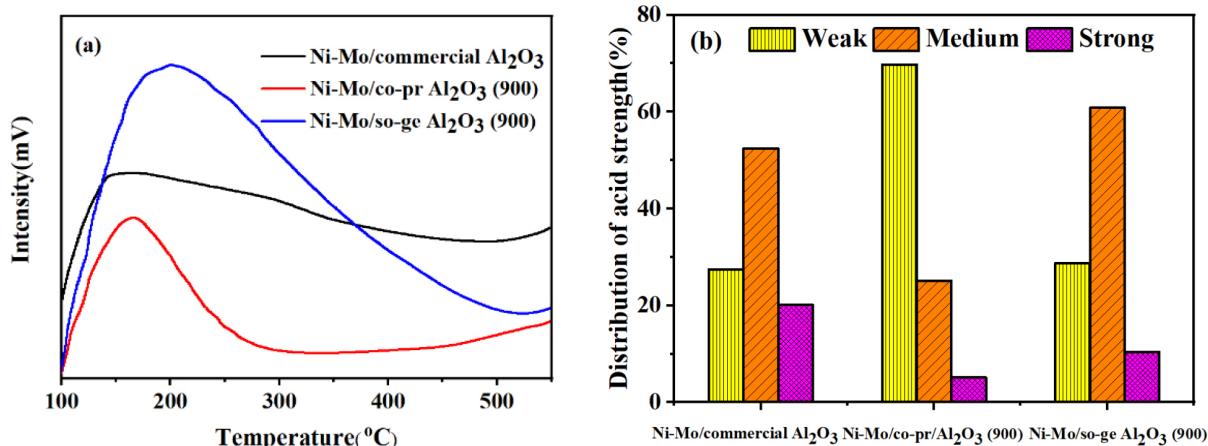


Figure 3. NH<sub>3</sub>-TPD curves (a) and acid strength distribution (b) of different Ni-Mo/Al<sub>2</sub>O<sub>3</sub> catalysts.

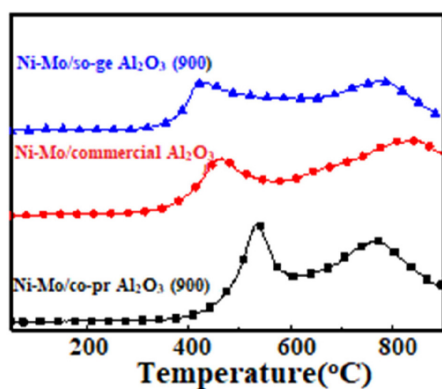


Figure 4. H<sub>2</sub>-TPR profiles of different Ni-Mo/Al<sub>2</sub>O<sub>3</sub> catalysts.

respectively.<sup>28</sup> The lower peak temperatures of Ni-Mo/so-ge Al<sub>2</sub>O<sub>3</sub>, Ni-Mo/commercial Al<sub>2</sub>O<sub>3</sub> and Ni-Mo/co-pr Al<sub>2</sub>O<sub>3</sub> were 430, 480 and 540 °C, respectively.

#### Catalytic performance

Table 3 presents the catalytic performances of different Ni-Mo/Al<sub>2</sub>O<sub>3</sub> catalysts. For Ni-Mo/co-pr Al<sub>2</sub>O<sub>3</sub>, naphthalene conversion and tetralin selectivity first increased and then

Table 3. Catalytic performances of different Ni-Mo/Al<sub>2</sub>O<sub>3</sub> catalysts

Catalyst	Naphthalene		Tetralin	
	Conversion / %	Selectivity / %	Yield / %	
Ni-Mo/commercial Al <sub>2</sub> O <sub>3</sub>	95.62	99.75	95.38	
Ni-Mo/co-pr Al <sub>2</sub> O <sub>3</sub> (600)	1.02	38.67	0.39	
Ni-Mo/co-pr Al <sub>2</sub> O <sub>3</sub> (700)	1.61	75.28	1.21	
Ni-Mo/co-pr Al <sub>2</sub> O <sub>3</sub> (800)	21.33	97.56	20.81	
Ni-Mo/co-pr Al <sub>2</sub> O <sub>3</sub> (900)	9.49	94.10	8.93	
Ni-Mo/so-ge Al <sub>2</sub> O <sub>3</sub> (800)	99.90	10.46	10.45	
Ni-Mo/so-ge Al <sub>2</sub> O <sub>3</sub> (900)	99.56	99.43	98.99	
Ni-Mo/so-ge Al <sub>2</sub> O <sub>3</sub> (1000)	99.49	75.60	75.21	
Ni-Mo/so-ge Al <sub>2</sub> O <sub>3</sub> (1100)	93.48	93.28	87.20	

decreased with increasing calcination temperature. Among the Ni-Mo/co-pr Al<sub>2</sub>O<sub>3</sub> catalysts, Ni-Mo/co-pr Al<sub>2</sub>O<sub>3</sub> (800) has the highest catalytic activity, achieving 21.33% naphthalene conversion, 97.56% tetralin selectivity and 20.81% tetralin yield, respectively, which may be due to the  $\gamma$  phase of Al<sub>2</sub>O<sub>3</sub> prepared at 800 °C. Compared with Ni-Mo/co-pr Al<sub>2</sub>O<sub>3</sub>, Ni-Mo/so-ge Al<sub>2</sub>O<sub>3</sub> catalysts show better catalytic performance. The conversions of naphthalene are greater than 93% for all Ni-Mo/co-pr Al<sub>2</sub>O<sub>3</sub> catalysts. Meanwhile, Ni-Mo/so-ge Al<sub>2</sub>O<sub>3</sub> (900) has the highest catalytic activity, achieving 99.56% naphthalene conversion, 99.43% tetralin selectivity and 98.99% tetralin yield, respectively. Furthermore, compared with Ni-Mo/commercial Al<sub>2</sub>O<sub>3</sub>, naphthalene conversion and tetralin selectivity of Ni-Mo/so-ge Al<sub>2</sub>O<sub>3</sub> (900) were increased by 4.12 and 3.78%, respectively.

#### Conclusions

In conclusion, Ni-Mo/commercial Al<sub>2</sub>O<sub>3</sub>, Ni-Mo/co-pr Al<sub>2</sub>O<sub>3</sub> and Ni-Mo/so-ge Al<sub>2</sub>O<sub>3</sub> catalysts were prepared for the selective hydrogenation of naphthalene to high-value tetralin.

The optimal Al<sub>2</sub>O<sub>3</sub> support was the pure  $\gamma$  phase, while the  $\theta$  and  $\alpha$  Al<sub>2</sub>O<sub>3</sub> phases were unfavorable for good catalytic performance. The largest S<sub>BET</sub> and proper pore size of the Ni-Mo/so-ge Al<sub>2</sub>O<sub>3</sub> (900) product may be the main reasons for its better catalytic performance. In the obtained catalysts, Ni-Mo/so-ge Al<sub>2</sub>O<sub>3</sub> (900) has shown the best catalytic performance with 99.56% naphthalene conversion, 99.43% tetralin selectivity and 98.99% tetralin yield, respectively.

## Acknowledgments

The authors are grateful for financial support from the Fundamental Research Funds for the Central Universities (31920220031, 31920220032), the Department of Education of Gansu Province: Young Doctor Fund Project (2022QB-029), the Scientific Research Project of Introducing Talents of Northwest Minzu University (xbmuyjrc202215, xbmuyjrc202216), and the Key Research and Development Project of Gansu Province (21YF5GA061).

## Author Contributions

Xiao-Ping Su was responsible for conceptualization, data curation, formal analysis, funding acquisition, investigation, methodology, project administration, writing original draft, review and editing; Le Zhao for resources; Xiang-Tong Wang for data curation; Zhao Wang for supervision; Zhi-Chao Wang for software; Tao Shen for formal analysis; Ping Zhang for funding acquisition.

## References

- Liu, J. J.; Zhang, H. F.; Lu, N. Y.; Yan, X. L.; Fan, B.; Li, R.; *Ind. Eng. Chem. Res.* **2020**, *59*, 1056. [Crossref]
- Li, P. F.; Wang, L.; Zhang, X. W.; Li, G. Z.; *ChemistrySelect* **2021**, *6*, 5524. [Crossref]
- Escobar, J.; Barrera, M. C.; Santes, V.; Terrazas, J. E.; *Catal. Today* **2017**, *296*, 197. [Crossref]
- Ardakani, S. J.; Smith, K. J.; *Appl. Catal., A* **2011**, *403*, 36. [Crossref]
- Liu, X. B.; Ardakani, S. J.; Smith, K. J.; *Catal. Commun.* **2011**, *12*, 454. [Crossref]
- Lee, J.; Choi, Y.; Shin, J.; Lee, J. K.; *Catal. Today* **2016**, *265*, 144. [Crossref]
- Bykov, A. V.; Alekseeva, D. V.; Demidenko, G. N.; Vasiliev, A. L.; Nikoshvili, L.; Kiwi-Minsker, L.; *Catalysts* **2020**, *10*, 1362. [Crossref]
- Guan, W. B.; Zhao, B. X.; Gao, H.; Hu, N. N.; Zhao, X. L.; *Catal. Commun.* **2017**, *98*, 57. [Crossref]
- Kostyniuk, A.; Bajec, D.; Likozar, B.; *Appl. Catal., A* **2021**, *612*, 118004. [Crossref]
- Li, F.; Yi, X. D.; Zheng, J. B.; Jin, H.; Fang, W. P.; *Catal. Commun.* **2009**, *11*, 266. [Crossref]
- Niu, B.; Jin, L. J.; Li, Y.; Shi, Z. W.; Li, Y. T.; Hu, H. Q.; *Fuel Process. Technol.* **2017**, *160*, 130. [Crossref]
- Hao, P.; Bai, Z.-Q.; Zhao, Z.-T.; Yan, J.-C.; Li, X.; Guo, Z.-X.; Xu, J.-L.; Bai, J.; Li, W.; *Fuel Process. Technol.* **2017**, *159*, 153. [Crossref]
- Sun, M.; Zhang, D.; Yao, Q. X.; Liu, Y. Q.; Su, X. P.; Jia, C. Q.; Hao, Q. Q.; Ma, X. X.; *Energy Fuels* **2018**, *32*, 7404. [Crossref]
- Cheng, Y.; Fan, H. L.; Wu, S. X.; Wang, Q.; Guo, J.; Gao, L.; Zong, B. N.; Han, B. X.; *Green Chem.* **2009**, *11*, 1061. [Crossref]
- Gong, P. Y.; Li, B. S.; Kong, X. L.; Liu, J. J.; Zuo, S. L.; *Appl. Surf. Sci.* **2017**, *423*, 433. [Crossref]
- Su, X. P.; An, P.; Gao, J. W.; Wang, R. C.; Zhang, Y. J.; Li, X.; Zhao, Y. K.; Liu, Y. Q.; Ma, X. X.; Sun, M.; *Chin. J. Chem. Eng.* **2020**, *28*, 2566. [Crossref]
- Budiman, A.; Ridwan, M.; Kim, S. M.; Choi, J.-W.; Yoon, C. W.; Ha, J. M.; D. Suh, J.; Suh, Y.-W.; *Appl. Catal., A* **2013**, *462*, 220. [Crossref]
- Zangouei, M.; Moghaddam, A. Z.; Arasteh, M.; *Chem. Eng. Res. Bull.* **2010**, *14*, 97. [Crossref]
- Ergazieva, G. E.; Telbayeva, M. M.; Popova, A. N.; Ismagilov, Z. R.; Dossunov, K.; Myltybayeva, L. K.; Dodinov, V. G.; Sozinov, S. A.; Niyazbayeva, A. I.; *Chem. Pap.* **2021**, *75*, 2765. [Crossref]
- Sun, R. J.; Shen, S. G.; Zhang, D. F.; Ren, Y. P.; Fan, J. M.; *Energy Fuels* **2015**, *29*, 7005. [Crossref]
- Liu, R.; Elleuch, O.; Wan, Z. Y.; Zuo, P.; Janicki, T. D.; Alfieri, A. D.; Babcock, S. E.; Savage, D. E.; Schmidt, J. R.; Evans, P. G.; Kuech, T. F.; *ACS Appl. Mater. Interfaces* **2020**, *51*, 57598. [Crossref]
- Kovarik, L.; Bowden, M.; Andersen, A.; Jaegers, N. R.; Washton, N.; Szanyi, J.; *Angew. Chem., Int. Ed.* **2020**, *59*, 21719. [Crossref]
- Huang, J. S.; Chen, C. L.; Huang, Z. L.; Fu, J. R.; Chen, S.; Jiang, Y. A.; Lu, L.; Xia, Y.; Zhao, X.; *Ceram. Int.* **2021**, *47*, 16943. [Crossref]
- Huang, Z.; Li, H.-S.; Miao, H.; Guo, Y.-h.; Teng, L.-j.; *Chem. Eng. Res. Des.* **2014**, *92*, 1371. [Crossref]
- Zhao, W.; Li, J. J.; He, C.; Wang, L. N.; Chu, J. L.; Qu, J. K.; Qi, T.; Hao, Z. P.; *Catal. Today* **2010**, *158*, 427. [Crossref]
- Sánchez-Minero, F.; Ramírez, J.; *Ind. Eng. Chem. Res.* **2011**, *50*, 2671. [Crossref]
- Kumar, R.; Kumar, K.; Choudary, N. V.; Pant, K. K.; *Fuel Process. Technol.* **2019**, *186*, 40. [Crossref]
- Zhang, S. S.; Ying, M.; Yu, J.; Zhang, W. C.; Wang, L.; Y. Guo, Y.; Guo, L.; *Appl. Catal., B* **2021**, *291*, 120074. [Crossref]

Submitted: June 21, 2022

Published online: January 17, 2023

